ACS APPLIED MATERIALS & INTERFACES

Forum Article

www.acsami.org

Improved Field-Effect Transistor Performance of a Benzotrithiophene Polymer through Ketal Cleavage in the Solid State

Christian B. Nielsen,*[,†] Eun-Ho Sohn,*[,‡] Dong-Jun Cho,[‡] Bob C. Schroeder,[†] Jeremy Smith,[§] Mongryong Lee,[‡] Thomas D. Anthopoulos,[§] Kigook Song,[‡] and Iain McCulloch[†]

[†]Department of Chemistry and Centre for Plastic Electronics, Imperial College London, London SW7 2AZ, United Kingdom

[‡]Kyung Hee University, Yongin, Gyeonggi-do 446-701, Korea

[§]Department of Physics and Centre for Plastic Electronics, Imperial College London, London SW7 2AZ, United Kingdom

Supporting Information

ABSTRACT: A benzotrithiophene polymer with a new thermally cleavable ketal substituent is reported. It is shown how this functional group can be used to facilitate solvent processing and, subsequently, how it can be removed by a thermal annealing process to generate a structurally ordered and crystalline thin film with significantly improved field-effect transistor properties.

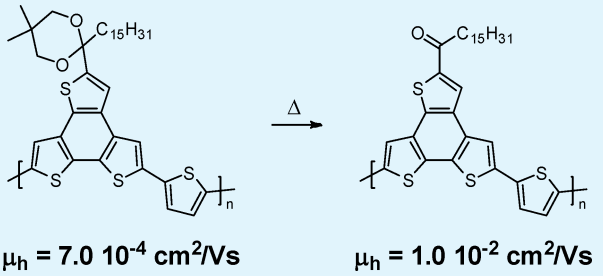

KEYWORDS: *benzotrithiophene, field-effect transistors, conjugated polymers, thermal cleavage, hole mobility*

INTRODUCTION

The research into π-conjugated organic semiconducting materials for organic electronic applications such as field-effect transistors (FETs) is progressing rapidly. Recently, thiophene-based polymers have shown hole mobilities above 1 $cm^2/(V\ s)$, while thiophene- and 2,1,3-benzothiadiazole-containing polymers have afforded hole mobilities in excess of 3 $cm^2/(V\ s)$.[1−3] The design of new high-performing thiophene-based semiconductors is generally focused on maximizing backbone planarity and interchain interactions to facilitate intramolecular and intermolecular charge transport. This effort must be closely counterbalanced by the introduction of solubilizing alkyl chains to aid solubility and processability without disrupting the solid-state packing. In this context, long linear alkyl chains are typically found to give superior FET performance; however, for large fused aromatic units with strong intermolecular interactions, a higher alkyl chain density, or steric inhibition to close packing in the form of branched alkyl chains, is often needed. It has recently been shown that the location of the alkyl chain branching point in relation to the polymer backbone can affect the FET performance drastically.[4] Moving the branching point away from the polymer backbone allows for better π-stacking and, therefore, better charge transport, but at the same time, the solubility-enhancing effect of the alkyl branching is greatly reduced. Here, we introduce a new approach using the ketone/ketal interconversion to create a soluble and easily processable ketal-functionalized semiconducting polymer that can subsequently be converted to the planar ketone form in the solid state to improve the packing and structural order and, therefore, the charge carrier mobility.[5]

We have previously shown that benzo[1,2-b:3,4-b′:5,6-d″]trithiophene (BTT) holds promise for organic FET applications with a branched 1-octylnonyl-functionalized BTT monomer copolymerized with thiophene (T) and thienothiophene (TT), affording polymers with hole mobilities above 0.2 $cm^2/(V\ s)$.[6] We have furthermore shown that ketalization of acyl-functionalized BTT-containing polymers can greatly increase the solubility.[7] These results prompted us to further investigate a ketal-functionalized BTT-T copolymer and we show herein that a simple thermal treatment in the solid state can convert this soluble and easily processable polymer with a high alkyl density to the corresponding ketone-functionalized BTT-T copolymer, which shows a much more ordered solid-state packing and a significantly increased FET hole mobility.

RESULTS AND DISCUSSION

Polymer Synthesis and Thermal Cleavage. Synthesis of the ketal-functionalized BTT-T polymer (**P1**, depicted in Scheme 1) was carried out in a fashion similar to that used for our previously reported BTT-T polymer, utilizing a Stille coupling between the dibrominated BTT monomer and the distannylated thiophene unit.[7] The crude polymer was purified by Soxhlet extractions with methanol, hexane, and dichloromethane, and **P1** was obtained thereafter via extraction with

Special Issue: Forum on Advancing Technology with Organic and Polymer Transistors

Received: December 17, 2012
Accepted: February 4, 2013
Published: February 4, 2013

ACS Publications © 2013 American Chemical Society

dx.doi.org/10.1021/am303138q | ACS Appl. Mater. Interfaces 2013, 5, 1806−1810

Scheme 1. Ketal-Functionalized BTT-T Polymer (P1) and Its Ketone Derivative (P2)

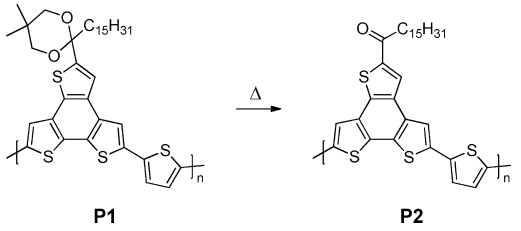

P1 P2

chloroform and subsequent precipitation into methanol. Gel permeation chromatography (GPC) in chlorobenzene at 80 °C (see Figure S1 in the Supporting Information (SI)) revealed a bimodal distribution ascribed to fully dissolved polymer and polymer aggregates. This was even observed for the lower-molecular-weight dichloromethane fraction, and it is clear that these strong aggregation tendencies hinder an accurate molecular weight determination of **P1**. When subject to thermogravimetric analysis in a nitrogen atmosphere with a heating rate of 10 °C/min, **P1** shows good thermal stability with <1% weight loss observed at 270 °C, as illustrated in Figure 1. Upon further heating from 270 °C to 300 °C, a very

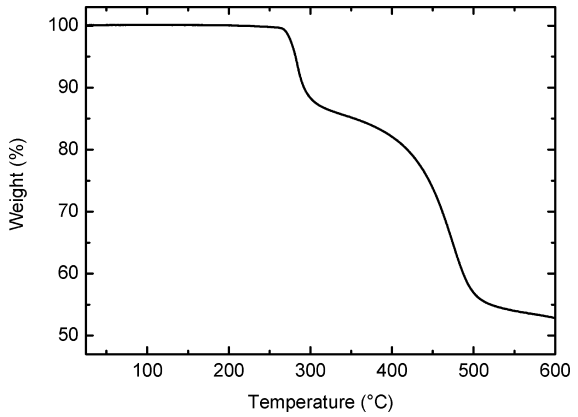

Figure 1. Thermogravimetric analysis trace for **P1** at a heating rate of 10 °C/min under nitrogen.

distinct thermal event takes place, and we note that the total weight loss of 12% at 300 °C is in excellent agreement with the theoretical weight loss of 13% when converting **P1** to **P2**. Further heating of the sample from 300 °C to 600 °C sees the material decompose gradually, with a final weight loss nearing 50% at 600 °C.

Spectroscopic Studies. The ultraviolet−visible light (UV-vis) absorption spectrum of **P1** in dilute *o*-dichlorobenzene (ODCB) is presented in Figure 2A. The absorption maximum was found at 530 nm, with a second prominent peak at 573 nm and a small shoulder below 500 nm. It is clear from the temperature-dependent UV-vis study also presented in Figure 2A that the two major absorption bands in the 500−600 nm range are both from polymer aggregates as the bands are reduced in intensity with increasing temperature. This is further emphasized in Figure 2B, which depicts the difference spectra as the temperature is increased from 15 °C. From the difference spectra, it is clearer that the dissolution of aggregates is associated with the emergence of an absorption band with a maximum at 466 nm from fully dissolved **P1**. In view of the distinct weight loss observed by TGA indicating cleavage of the

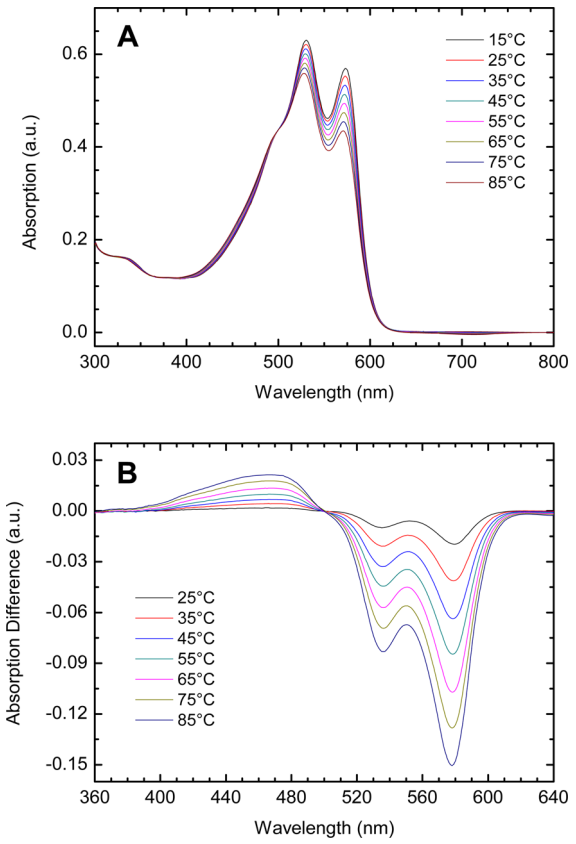

Figure 2. Temperature-dependent UV-vis absorption spectra (A) and the corresponding difference spectra (B) for an *o*-dichlorobenzene solution of **P1**.

ketal, a thin spin-cast film of **P1** was furthermore investigated using UV-vis (Figure 3) and Fourier transform infrared (FTIR;

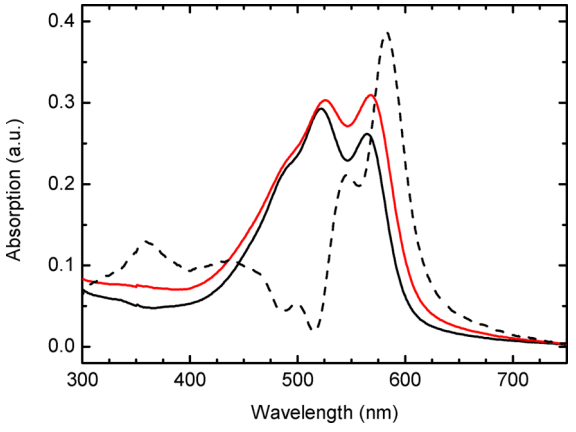

Figure 3. UV−vis absorption spectra for a thin film of **P1** before (black line) and after (red line) thermal annealing at 350 °C for 10 min; the dashed line represents the magnified (3×) difference spectrum between the two thin films.

see Figure 4) spectroscopy before and after thermal annealing at 350 °C for 10 min. The pristine film of **P1** before thermal annealing is slightly blue-shifted, relative to the solution spectrum, with peaks at 522 and 565 nm. Thermal annealing affords a slightly red-shifted spectrum and an increase in the low-energy peak (568 nm), relative to the high-energy peak (526 nm), which is indicative of a more ordered film. Upon

dx.doi.org/10.1021/am303138q | *ACS Appl. Mater. Interfaces* 2013, 5, 1806−1810

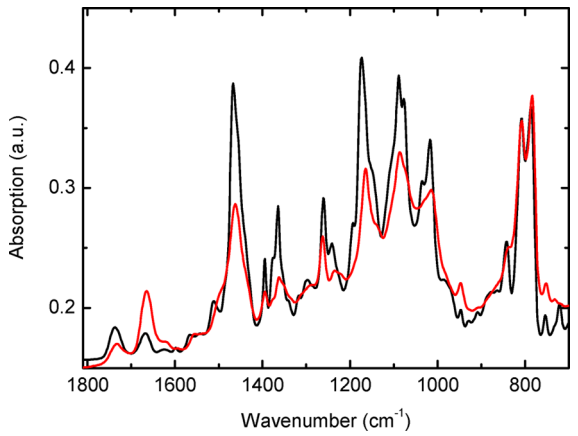

Figure 4. Fourier transform infrared (FTIR) spectra for a thin film of **P1** before (black line) and after (red line) thermal annealing at 350 °C for 10 min.

closer inspection of the difference spectrum, we also note a significant increase in an absorption feature at ~360 nm, which we ascribe to ketone formation, as will be discussed in more detail in the following. We furthermore note that the annealed thin film, in contrast to the as-cast film, remains intact after rinsing with chlorinated solvents such as chloroform or chlorobenzene; this observation further supports our hypothesis of ketal cleavage. Comparison of the FTIR spectra before and after annealing similarly indicates conversion of ketal (**P1**) to ketone (**P2**). Most notably, the C═O stretch observed at 1665 cm^{-1} gives a strong indication of ketone formation. In the 1500−1300 cm^{-1} region, bands are typically ascribed to CH_2 and CH_3 (asymmetric) bending (1470−1460 cm^{-1}) and symmetric CH_3 bending (1400−1360 cm^{-1}), and we note a decrease of intensity in this region upon annealing in agreement with loss of the CH_2− and CH_3-rich neopentyl group. Ketals typically give rise to three C−O stretching bands in the 1200−1000 cm^{-1} region,[8] and again we observe a decrease in intensity in this region congruent with the hypothesized ketal cleavage. When the thermal annealing time was increased from 10 min to 20 min, no further changes were observed in either the UV-vis or the FTIR spectra, suggesting that sufficient time had been allowed for full ketal-defunctionalization to take place.

Field-Effect Transistor Performance. To investigate the effect of the solid-state conversion of the ketal-functionalized BTT-T polymer (**P1**) to the corresponding ketone (**P2**) on charge-carrier mobility, bottom-gate/top-contact field-effect transistor (FET) devices were fabricated. **P1** was deposited onto hexamethyldisilazane-treated Si/SiO_2 substrates by spin-coating from chlorobenzene and subsequently preheated for 2 h at 150 °C to remove residual solvents. Gold electrodes were subsequently deposited on top via thermal evaporation. The output and transfer characteristics of the devices are depicted in Figure 5. The FET device with as-cast **P1** showed a saturated hole mobility of 7.0×10^{-4} $cm^2/(V\ s)$ with an on/off ratio of 10^3 and a threshold voltage of −23.9 V. Upon thermal annealing at 350 °C—and, consequently, conversion of **P1** to **P2**—a significantly improved hole mobility of 1.0×10^{-2} $cm^2/(V\ s)$ and a higher on/off ratio of 10^4 was measured for the FET device, while the threshold voltage was shifted to −29.5 V. This nearly 15-fold increase in hole mobility upon annealing nicely corroborates our hypothesis that a large fraction of the bulky neopentyl groups of **P1** are cleaved off to afford a much less bulky side-chain (**P2**) and thus facilitate backbone

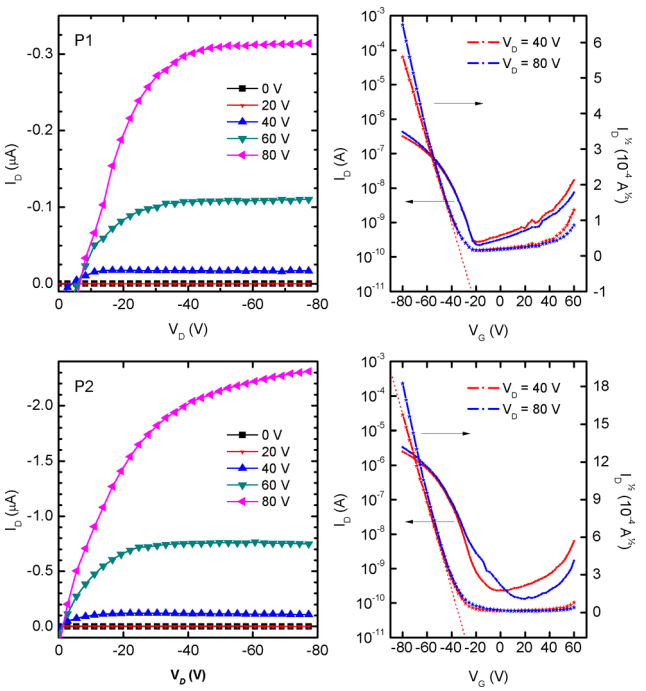

Figure 5. Output (left) and transfer (right) characteristics of a **P1** field-effect transistor (FET) device before (top) and after (bottom) thermal annealing at 350 °C.

planarization and a tighter packing in the solid state and, therefore, much improved intramolecular and intermolecular charge transport. The observed larger negative gate voltage required to initiate hole conduction upon thermal annealing (−29.5 V vs −23.9 V) is in agreement with effective ketal cleavage, because the formation of the electron-withdrawing ketone functionality indisputably will deepen the highest occupied molecular orbital (HOMO) of the BTT-T polymer.[9]

Morphological Studies. We subsequently employed atomic force microscopy (AFM) and grazing incidence X-ray diffraction (GIXD) to probe the surface morphology and the bulk morphology, respectively, of the thin films before and after thermal ketal defunctionalization. As illustrated in Figure 6, the AFM images reveal a homogeneous and fairly smooth surface morphology (root-mean-square (RMS) roughness of 0.91 nm) for the as-cast thin film of **P1**. After thermal annealing, on the other hand, two different phases are clearly present in both the phase and the topography image, which we ascribe to the partial formation of ketone polymer **P2**. Individually, the two phases appear very smooth, but because of the height difference between the two phases, the RMS roughness of the annealed film is increased slightly, to 1.07 nm. The GIXD patterns presented in Figure 7 indicate lamellar packing perpendicular to the surface for both films and, thus, an edge-on orientation of the conjugated plane, as seen for most high-mobility polymers.[10] For the as-cast film of **P1**, a lamellar repeat unit of 29.0 Å is found, whereas the annealed film (**P2**) shows a slightly reduced lamellar *d*-spacing of 28.3 Å, in agreement with the loss of alkyl chain density upon ketal cleavage, as well as the more favorable packing indicated by UV-vis spectroscopy and FET device characteristics. Moreover, the out-of-plane one-dimensional GIXD plots (Figure 7c) clearly show that the degree of crystallinity is significantly increased upon the conversion of **P1** to **P2**, which again corroborates efficient

dx.doi.org/10.1021/am303138q | ACS Appl. Mater. Interfaces 2013, 5, 1806−1810

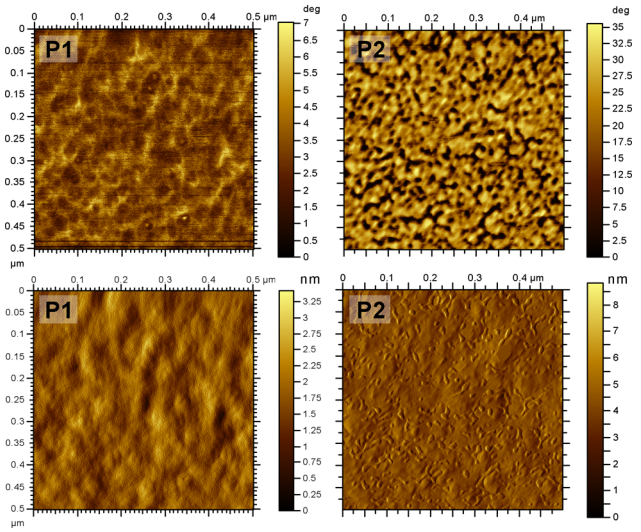

Figure 6. Close-contact atomic force microscopy (AFM) micrographs (0.5 μm × 0.5 μm) of **P1** (left) and **P2** (right) showing the phase (top) and topographic (bottom) contrast.

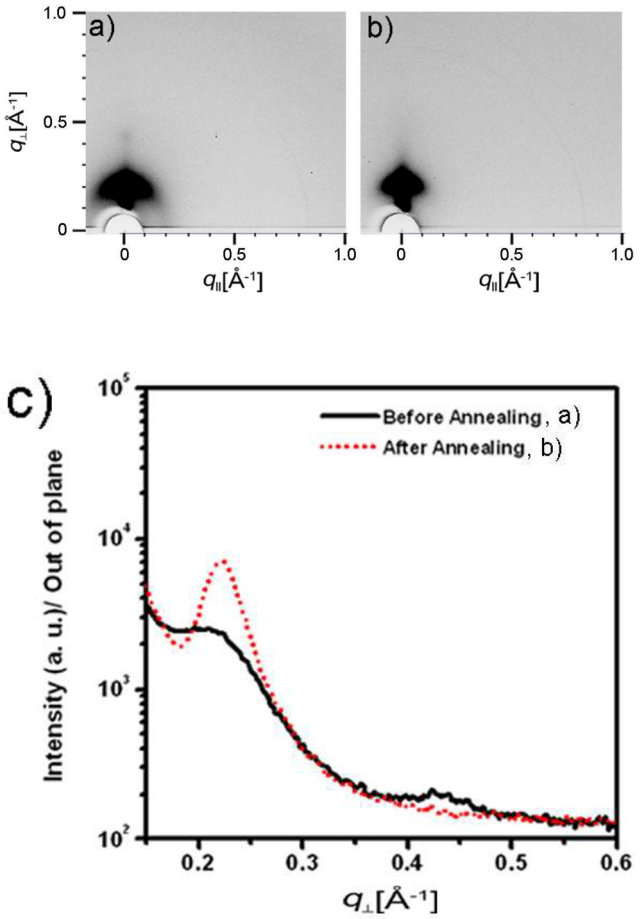

Figure 7. Two-dimensional (2D) grazing incidence X-ray diffraction (GIXD) diffractograms of (a) an as-cast thin film of **P1** and (b) the film after thermal annealing (**P2**). Panel (c) shows the out-of-plane one-dimensional (1D) GIXD plot for the two samples.

ketal cleavage and thus backbone planarization and interchain ordering.

Small Molecule Model System. To further test our hypothesis of thermal ketal cleavage in the solid state without the aid of water or acid catalysis, we synthesized the two small molecules depicted in Scheme 2. Compound **1** is a ketone-functionalized BTT unit flanked by two 3-hexylthiophene units, and compound **2** is the corresponding ketal obtained by the acid-catalyzed reaction with neopentyl glycol. The small molecule model system is designed to resemble the BTT-T polymers studied herein (**P1** and **P2**) and yet be fully soluble both in the ketone and the ketal form in order to allow a more accurate chemical analysis. Infrared (IR) spectra of **1** and **2** that are included in the SI (Figure S2) confirm our IR peak assignments discussed above and UV-vis spectra of **1** and **2** (see Figure S4 in the SI) similarly verify that the absorption band at ~360 nm can be attributed to the ketone-functionalized BTT moiety. Computational modeling (Gaussian at the B3LYP/6-31G* level) indicate that the additional absorption band can be ascribed to the HOMO-1 → LUMO transition, which has a nearly 50-fold higher oscillator strength for **1**, compared to **2**. Visualization of the frontier orbital distributions (see Figure S5 in the SI) shows a good overlap of the HOMO-1 and LUMO orbitals for compound **1** and much less so for compound **2**. Moreover, taking advantage of the good solubility of both model compounds, a neat 70:30 molar mixture of **1** and **2** was heated to 300 °C for 10 min in an argon atmosphere to mimic the thin film annealing conditions. Nuclear magnetic resonance (NMR) spectra before and after this thermal treatment, as depicted in Figure 8, unambiguously show that the ketone content (**1**) is increased at the expense of the acetal (**2**) corroborating the thermal conversion of **2** to **1**, as also suggested in Scheme 2.

Scheme 2. Ketone and Ketal Model Compounds 1 and 2

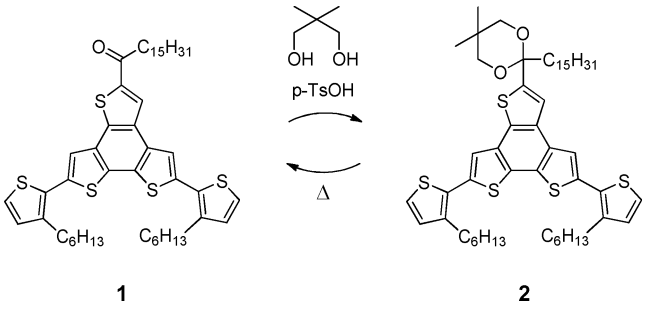

Proposed Cleavage Mechanism. As illustrated in Scheme 3 (top), the classical ketal deprotection is typically carried out in the presence of acid and water to afford the corresponding ketone and diol. In this work, we have clearly illustrated that the ketal defunctionalization of both polymer **P1** and small molecule model compound **2** takes place in the solid state without the aid of acid or water. Therefore, we propose the alternative cleavage mechanism presented in Scheme 3 (bottom), which can be seen as a pericyclic rearrangement driven by the formation of the ketone and the highly volatile byproducts isobutene and formaldehyde. Although we believe this mechanism to be highly plausible, we stress that this is speculative at the moment. Further mechanistic investigations must be carried out to verify this hypothesis.

CONCLUSIONS

In conclusion, we have introduced a new thermally cleavable side group and shown how this labile ketal moiety can be used to facilitate good solubility and processability in π-conjugated polymers. Subsequent thermal cleavage can easily be realized

dx.doi.org/10.1021/am303138q | ACS Appl. Mater. Interfaces 2013, 5, 1806−1810

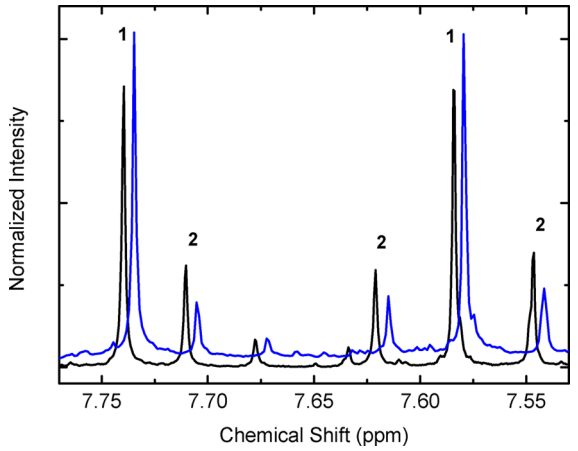

Figure 8. Section of the ^{1}H NMR spectra of a 70:30 molar mixture of **1** and **2** before (black line) and after (blue line) heating to 300 °C for 10 min in an argon atmosphere; the spectrum after heating is offset slightly for clarity. The two singlets from the BTT moiety in **1** are observed at 7.74 and 7.58 ppm (a third singlet is observed at 8.32 ppm), while the three singlets from the BTT moiety in **2** are found at 7.71, 7.62, and 7.55 ppm.

Scheme 3. Conventional Acid-Catalyzed Hydrolysis of a Ketal (top) and Proposed Thermal Cleavage Reaction of Ketal (bottom)

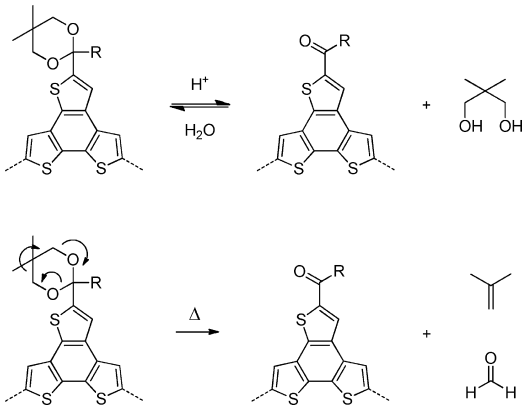

through a simple annealing step that only generates highly volatile side products, which can easily escape a thin film. The beneficial structural ordering associated with the thermal cleavage was verified by a significant increase in crystallinity and, more importantly, by a large increase in FET hole mobility (by more than 1 order of magnitude). This clearly highlights the potential of this new approach as a promising tool for the continued development of high-performing π-conjugated semiconducting materials. We furthermore believe that this new and straightforward side-chain defunctionalization approach could be very useful for practical patterning applications, and detailed studies hereof are currently underway in our laboratories.

■ ASSOCIATED CONTENT

Supporting Information

Experimental details, GPC chromatograms, IR spectra, UV-vis spectra, and images of frontier molecular orbital distributions. This information is available free of charge via the Internet at http://pubs.acs.org.

■ AUTHOR INFORMATION

Corresponding Author

*E-mail: c.nielsen@imperial.ac.uk (C.B.N.); inseh98@khu.ac.kr (E.-H.S.).

Notes

The authors declare no competing financial interest.

■ ACKNOWLEDGMENTS

This work was in part carried out with financial support from SUPERGEN, EC FP7 Project X10D, EC FP7 Project ONE-P, EPSRC (No. EP/G037515/1), and the International Collaborative Research Program of Gyeonggi-do, Korea.

■ REFERENCES

(1) Zhang, W.; Smith, J.; Watkins, S. E.; Gysel, R.; McGehee, M.; Salleo, A.; Kirkpatrick, J.; Ashraf, S.; Anthopoulos, T.; Heeney, M.; McCulloch, I. *J. Am. Chem. Soc.* **2010**, *132*, 11437.

(2) Kim, J.; Lim, B.; Baeg, K.-J.; Noh, Y.-Y.; Khim, D.; Jeong, H.-G.; Yun, J.-M.; Kim, D.-Y. *Chem. Mater.* **2011**, *23*, 4663.

(3) Tsao, H. N.; Cho, D. M.; Park, I.; Hansen, M. R.; Mavrinskiy, A.; Yoon, D. Y.; Graf, R.; Pisula, W.; Spiess, H. W.; Müllen, K. *J. Am. Chem. Soc.* **2011**, *133*, 2605.

(4) Lei, T.; Dou, J.-H.; Pei, J. *Adv. Mater.* **2012**, *24*, 6457.

(5) (a) Yu, J.; Holdcroft, S. *Macromolecules* **2000**, *33*, 5073. (b) Afzali, A.; Dimitrakopoulos, C. D.; Breen, T. L. *J. Am. Chem. Soc.* **2002**, *124*, 8812. (c) Afzali, A.; Dimitrakopoulos, C. D.; Graham, T. O. *Adv. Mater.* **2003**, *15*, 2066. (d) Murphy, A. R.; Frechet, J. M. J.; Chang, P.; Lee, J.; Subramanian, V. *J. Am. Chem. Soc.* **2004**, *126*, 1596. (e) Liu, J.; Kadnikova, E. N.; Liu, Y.; McGehee, M. D.; Fréchet, J. M. J. *J. Am. Chem. Soc.* **2004**, *126*, 9486. (f) Bjerring, M.; Nielsen, J. S.; Nielsen, N. C.; Krebs, F. C. *Macromolecules* **2007**, *40*, 6012.

(6) Schroeder, B. C.; Nielsen, C. B.; Kim, Y. J.; Smith, J.; Huang, Z.; Durrant, J.; Watkins, S. E.; Song, K.; Anthopoulos, T. D.; McCulloch, I. *Chem. Mater.* **2011**, *23*, 4025.

(7) Nielsen, C. B.; Fraser, J. M.; Schroeder, B. C.; Du, J.; White, A. J. P.; Zhang, W.; McCulloch, I. *Org. Lett.* **2011**, *13*, 2414.

(8) Socrates, G. *Infrared and Raman Characteristic Group Frequencies: Tables and Charts*; 3rd ed.; John Wiley & Sons Ltd: Chichester, U.K., 2001.

(9) Calculations using Gaussian at the B3LYP/6-31G* level predict HOMO levels of −5.12 eV for **P1** and −4.76 eV for **P2**.

(10) Nielsen, C. B.; Turbiez, M.; McCulloch, I. *Adv. Mater.* **2012**, DOI: 10.1002/adma.201201795.